SOLUTION OF THE NAVIER-STOKES EQUATIONS FOR THE FLOW AROUND AN AEROFOIL IN AN OSCILLATING FREE STREAM

Scott Shaw
Ning Qin

Cranfield College of Aeronautics,
Cranfield University,
Bedfordshire.
United Kingdom.

Abstract

This paper describes a method for the solution of the unsteady thin layer Navier-Stokes equations about aerofoils undergoing in-plane oscillations. The method has been used to study the development of the unsteady flowfield around a NACA 0012 aerofoil at flow conditions representative of rotor blades in high speed forward flight. In thi" s paper two cases are considered, in the first (which has a moderate advance ratio) calculated shock-boundary layer interactions are weak and fair comparison is found between calculation and experiment. In the second case (which has a higher advance ratio) calculations indicate that the flowfield is no longer symmetric for a range of azimuth angles following shock induced separation. This behaviour was not observed during experiments and consequently agreement between calculation and experiment is poorer. This phenomena is related to the occurrence of shock induced separation. It is possible that this behaviour is suppressed by three dimensional effects, which are not modelled, during rotor tests. In order to establish confidence in the present method calculated results are also presented for the steady flowfield around the RAE 2822 aerofoil and the self-excited periodic flow of a rigid 14% thick circular arc aerofoil.

Introduction

In principal the Navier-Stokes equations contain all of the necessary flow physics for the calculation of the flowfield around helicopter rotors in forward flight. However, despite significant progress in the last decade the accurate calculation of such flows remains beyond the current capabilities of computational fluid dynamics.

The problems which arise in calculating the flowfield around helicopter rotors may be broadly categorised as retreating blade dynamic stall, advancing blade compressibility effects and the production, convection and interactions of vorticity in the rotor wake.

Dynamic stall is the unsteady separation at high lift coefficients associated with bodies performing time dependent motions. It is a process which is governed by complex flow physics including transition, separation and large scale vortex shedding in the proximity of lifting surfaces. Reviews of both experimental and computational progress in this field have been presented by Carr[1] and Carr and McCroskey[2]. Performance of a wide range of algebraic, one- and two-equation turbulence models was investigated by Ekaterinaris, Srinivasan and McCroskey[3]. It was found that none of the turbulence models tested were capable of predicting deep stall, although more recent turbulence models offered significant improvements over standard two-equation models. Transition from laminar to turbulent flow was also demonstrated to play an important role in the overall development of the unsteady flowfield. Recent experimental measurements[4] have shown that compressibility effects become important at moderate Mach numbers (0.3) and can promote the onset of dynamic stall.

Unlike fixed wing aircraft helicopter rotors operate within their own wake, an accurate treatment of the rotor wake is therefore critical for reliable performance prediction. Non-physical dissipation of vorticity, as a result of numerical approximation of the Navier-Stokes equations, represents the most important obstacle to the accurate calculation of the rotor wake system. McCroskey has reviewed progress in the measurement and prediction of rotor wakes[5]. Recent work aimed at reducing non-physical dissipation of vorticity has concentrated on reducing the truncation error of the numerical approximations by grid refinement in areas of high vorticity[6,7] and the use of higher order difference schemes[8,9]. An alternative approach, vorticity confinement, has been proposed by Steinhoff [10] in which a self-interaction term is added to the momentum equations. This additional term depends on the local velocity and prevents numerical diffusion by convecting vorticity back towards the vortex core.

Since the pioneering experiments of Tijdemann[11] in the mid 1970's there has been great interest in the development of computational methods for the analysis of unsteady shock-boundary layer interactions. Recent work in this field was comprehensively reviewed by Edwards and Thomas[12]. Experimental investigations of self-excited periodic flows have been reported by McDevitt et al[13] and Mabey et al[14] for 14% and 18% thick bi-convex circular arc aerofoils. Levy's[15] solutions of the Navier-Stokes equations for these aerofoils qualitatively reproduced the oscillatory trailing edge/shock induced separations observed in the experiments. More recently Rumsey et al[16] have performed calculations using a one-equation turbulence model for an 18% thick circular arc aerofoil. The scale and frequency of the calculated oscillations show good agreement with experiment.

In forward flight the motion of the rotor blade in the plane of the rotor disc can be represented by an aerofoil oscillating in translation. Favier et al[17-19] have investigated the influence of this motion at low free stream velocities in isolation and when coupled with pitching oscillations. Analytical expressions for the lift transfer function have been obtained by Van der Wall and Leishman[20] for incompressible flow which show good agreement with incompressible Euler calculations. In the transonic flow regime Lerat and Sides[21] examined in-plane oscillations with the Euler equations with some success. More recently Habibie, Laschka and Weishaupl[22] and Lin and Pahlke[23] have used the Euler equations to study translation, plunge and pitching oscillations.

At very high advance ratios the Euler equations do not provide an adequate representation of the flow physics due to the occurrence of strong shock-boundary layer interactions which have important consequences for the development of the unsteady flow. In the present work a finite volume method based upon Oshers flux difference splitting is used to solve the thin layer Navier-Stokes equations for the transonic flow around aerofoils undergoing in-plane oscillations. A turbulent contribution to viscosity is provided by the Baldwin-Lomax turbulence model. This method has been used to study the unsteady aerodynamics of a NACA 0012 aerofoil at flow conditions representative of the high speed forward flight of non-lifting helicopter rotors. Two cases were considered, in the first case weak shock-boundary layer interactions were observed, while in the second case much stronger interactions including shock induced separation occurred. In order to validate the current approach calculations were also performed for the steady transonic flow about the RAE 2822 aerofoil and the self-excited periodic flow of a 14% thick circular arc aerofoil.

Governing Equations

The Navier-Stokes equations express the conservation of mass, momentum and energy and may be written in integral form for curvilinear co-ordinates as,

$$\int_{\Omega}\frac{\partial Q}{\partial t}+\int_{S}\frac{\partial(E_i-E_v)}{\partial\xi}dS_\xi+\int_{S}\frac{\partial(F_i-F_v)}{\partial\eta}dS_\eta=0 \quad (1)$$

in which Ω is the domain of the control volume, S is the boundary of the control volume, Q is the vector of conserved variables, E_i and F_i are the convective flux vectors and E_v and F_v are the viscous flux vectors in the ξ and η directions respectively.

In this work the thin layer form of the Navier-Stokes equations are solved. Under the thin layer approximation derivatives in the tangential direction are neglected in the viscous flux terms. Equation (1) is unaltered and the flux vectors are given by,

$$E_i=\begin{pmatrix}\rho U\\ \rho uU+\xi_x P\\ \rho vU+\xi_y P\\ U(e+P)\end{pmatrix},\quad F_i=\begin{pmatrix}\rho V\\ \rho uV+\eta_x P\\ \rho vV+\eta_y P\\ V(e+P)\end{pmatrix} \quad (2a)$$

$$E_v=(0),\quad F_v=\frac{1}{Re}\begin{pmatrix}0\\ \mu a_1 u_\eta+\frac{\mu}{3}\eta_x a_2\\ \mu a_1 v_\eta+\frac{\mu}{3}\eta_y a_2\\ \mu a_1 a_3+\frac{\mu}{3}a_2\left(\eta_x u+\eta_y v\right)\end{pmatrix} \quad (2b)$$

here,

$$a_1=\eta_x^2+\eta_y^2$$
$$a_2=\xi_x^2+\xi_y^2$$
$$a_3=\frac{u^2+v^2}{2}+\frac{c_\eta^2}{Pr(\gamma-1)}$$

and ρ, u, v, P, c, Re, Pr are density, Cartesian components of velocity, pressure, speed of sound, Reynolds number and Prandtl number respectively. U and V are the contravariant velocities calculated from,

$$U=\xi_x u+\xi_y v$$
$$V=\eta_x u+\eta_y v \quad (2c)$$

Equation (1) is extended for moving bodies in the following manner. Consider the one dimensional continuity equation,

$$\frac{\partial \rho}{\partial t} + \frac{\partial (\rho u)}{\partial x} = 0 \qquad (3)$$

Integrating for a control volume whose boundaries move over time we obtain,

$$\int_{x(t_1)}^{x(t_2)} \frac{\partial \rho}{\partial t} dx + \int_{x(t_1)}^{x(t_2)} \frac{\partial (\rho u)}{\partial x} dx = 0 \qquad (4)$$

After differentiation of the first term with respect to time and some further manipulation Equation (4) may be rewritten in the following form,

$$\frac{d}{dt} \int_{x(t_1)}^{x(t_2)} \rho dx + \int_{x(t_1)}^{x(t_2)} \frac{\partial}{\partial x} \rho \left(u - \frac{dx}{dt} \right) dx = 0 \qquad (5)$$

in which $\frac{dx}{dt}$ is the velocity with which the control volume surface moves, referred to as the grid velocity. Similar results follow for the momentum and energy equations.

This analysis shows that the governing equations may be rewritten for moving bodies by replacing the velocity in the convective flux terms (Equations (2a)) with the relative velocity of the fluid with respect to the moving grid. The convective flux vectors become,

$$E_i = \begin{pmatrix} \rho U \\ \rho u U + \xi_x P \\ \rho v U + \xi_y P \\ U(e+P) + \xi_t P \end{pmatrix}, F_i = \begin{pmatrix} \rho V \\ \rho u V + \eta_x P \\ \rho v V + \eta_y P \\ V(e+P) + \eta_t P \end{pmatrix} \qquad (6a)$$

in which the contravariant velocities are now calculated from,

$$\begin{aligned} U &= \xi_x \left(u - \frac{dx}{dt} \right) + \xi_y \left(v - \frac{dy}{dt} \right) \\ V &= \eta_x \left(u - \frac{dx}{dt} \right) + \eta_y \left(v - \frac{dy}{dt} \right) \end{aligned} \qquad (6c)$$

In the present work only rigid translations and rotations of the grid are considered.

Numerical procedure

Oshers flux vector splitting method[24] is employed for the spatial discretisation of the convective flux terms, Equations (6a). Higher order spatial accuracy is obtained using MUSCL interpolation together with a flux limiter. The viscous terms are discretised using central differences. The algebraic turbulence model proposed by Baldwin and Lomax is used to provide a turbulent contribution to the viscosity. It has been demonstrated by Qin[25] that such an approach captures both shock waves and shear layers accurately allowing the reliable prediction of shock-boundary interactions.

After spatial discretisation the governing equations are reduced to a system of ordinary differential equations which are integrated in time using a first order Euler implicit scheme. One implicit step of the method can be written as,

$$\left[I + \frac{\partial E_i}{\partial Q} + \frac{\partial F_i}{\partial Q} + \frac{\partial F_v}{\partial Q} \right] \frac{\partial Q}{\partial t} = -\Delta t \left(\frac{\partial E_i}{\partial \xi} + \frac{\partial F_i}{\partial \eta} + \frac{\partial F_v}{\partial \eta} \right) \qquad (7)$$

in which $\frac{\partial E_i}{\partial Q}$ and $\frac{\partial F_i}{\partial Q}$ are the inviscid flux Jacobians in the ξ- and η- directions respectively and $\frac{\partial F_v}{\partial Q}$ is the viscous flux Jacobian in the η-direction. The flux Jacobians are calculated using analytical expressions. While It is possible to obtain Jacobians for the Baldwin-Lomax turbulence model they do not exhibit a sparse structure. For this reason turbulent contributions to the flux Jacobian are neglected.

Equation (7) represents a sparse, system of linear equations of the form,

$$[A]\{x\} = \{b\} \qquad (8)$$

which can be solved using conjugate gradient methods. In this work restarted GMRES[26] is employed. The system of equations represented by Equation (8) are generally ill-conditioned which has severe consequences for the convergence of conjugate gradient methods.

In order to improve the condition of the system matrix, and hence the convergence behaviour of the linear solver, preconditioning is required. We seek a preconditioning matrix which when used to pre-multiply Equation (8) results in a new system of linear equations,

$$[C][A]\{x\}=[C]\{b\} \qquad (9)$$

which is more amenable to solution by iterative techniques. The preconditioner used in this work was proposed by Badcock and Richards[27]. They have demonstrated that a method based upon ADI factorisation provides a fast and effective preconditioner for the two-dimensional Navier-Stokes equations.

Results

The method described in the proceeding sections has been applied to the calculation of steady and unsteady flows for several aerofoils. Results of steady computations for the RAE 2822 aerofoil are presented which indicate the overall level of accuracy of the numerical scheme. The ability of the method to predict unsteady shock-boundary

layer interactions is demonstrated by calculation of the self-excited periodic flow which occurs for a rigid 14% thick bi-convex circular arc aerofoil at a freestream Mach number of 0.83. Finally calculations of the unsteady flowfield around a NACA0012 aerofoil undergoing in-plane motion are presented. Two cases are considered. In the first case there are weak shock boundary layer interactions while in the second there are much stronger interactions which include shock induced separation.

Steady flow around RAE 2822 aerofoil.

Steady state calculations were performed for the RAE 2822 aerofoil at a Mach number of 0.73, a Reynolds number of 6.5 million and an angle of attack of 2.79 degrees in order to establish the overall accuracy of the numerical method. Calculations were performed on a relatively coarse grid having 159 grid points in the streamwise direction (100 on the aerofoil surface) and 48 grid points in the normal direction. Calculated pressure distributions are compared with the experimental data of Cook et al[28] in Figure (1). The computations show good agreement with experiment over the entire aerofoil, although the location of the shock wave is slightly downstream of that observed in the wind tunnel tests. The calculated lift coefficient of 0.791 is in fair agreement with the experimental value of 0.803.

Self-excited periodic flow for a circular arc aerofoil

For a small range of Mach numbers close to the onset of shock induced separation Mabey[14] observed unsteady periodic flow on a 14% circular arc aerofoil. In order to validate the present method for unsteady flow, calculations were performed in free air for Mach numbers in the range 0.80 to 0.88, α = 0 degrees and a Reynolds number of 7 million. Transition between laminar and turbulent flow was fixed at 0.02 chord lengths from the leading edge. A relatively coarse grid containing 159 points in the streamwise direction and 48 points in the normal direction was employed.

The behaviour of calculated lift coefficient with non-dimensional time is presented in Figure (2) for a Mach number of 0.83. There is good agreement between the magnitude of the calculated oscillations and those of the experiment (which are indicated by the dashed lines). The calculated non-dimensional frequency of 1.21 is considerably higher than the measured frequency, which is approximately 1.0. The poor agreement of the calculated frequency parameter with experiment can be attributed in part to weaknesses in the algebraic turbulence model employed here. Ramsey et al[16] have demonstrated that more accurate predictions of the frequency parameter can be obtained using higher order turbulence models. Calculations of the unsteady flowfield at M=0.83 reproduce the characteristic oscillations between shock induced and trailing edge separation, see Figure (4), observed from experimental flow visualisation.

In the experiments of Mabey unsteady periodic flow was established at M=0.83 and persisted until M=0.86, this range of Mach numbers is indicated by the solid lines in Figure (3). The calculated onset Mach number for flow unsteadiness (M=0.82) and the range over which unsteadiness is observed are in fair agreement with those found in the experiment, see Figure (3). Previous calculations of the periodic flow around an 18% thick circular arc aerofoil indicate that the Mach numbers for which oscillatory flow is observed are sensitive to the inclusion of wind tunnel wall effects, see pages 249-250 of Edwards and Thomas[12], the present calculations were performed in free air.

Unsteady flow with no discernible period was also calculated over a much wider range of Mach numbers (0.8 to 0.88). This phenomena, which is of a much smaller scale than self-excited periodic flow, is caused by small random oscillations of the upper and lower surface shock waves and was also observed in the experiments.

The calculations detailed above demonstrate that the current numerical scheme is capable of predicting unsteady flow phenomena which arise as a consequence of shock-boundary layer interactions. Inconsistencies between calculation and experiment can largely be attributed to the neglection of wind tunnel wall effects and inadequacies in the algebraic turbulence model currently employed.

NACA 0012 aerofoil with in-plane motions.

The normal component of Mach number for a rotor blade section located a distance r from the axis of rotation is given by,

$$M_\infty = \frac{r}{R} M_{tip}\left(1+\mu \sin(\psi)\right) \qquad (10)$$

in which R is the radius of the rotor blade, M_{tip} is the tip Mach number in hover, μ is the ratio of forward flight speed to tip speed in hover (the advance ratio) and ψ is the azimuth angle. Neglecting three dimensional effects Equation (10) provides a basis for calculating the aerodynamics of helicopter rotor blades using the in-plane motions of aerofoils. Under this approximation the rotational speed of the rotor blade provides a mean flow velocity, $\frac{r}{R} M_{tip}$, while the forward flight speed can be represented by a grid velocity term,

$$\frac{dx}{dt} = \frac{r}{R} M_{tip} \mu^* \sin(kt) \qquad (11)$$

here, $\mu^* = \frac{R}{r}\mu$ and the reduced frequency, k, is obtained from,

$$k = \frac{\varpi c_{local}}{u_o} = \frac{\varpi c_{local}}{\varpi r} = \frac{c_{local}}{r} \qquad (12)$$

The aerodynamics of the NACA 0012 aerofoil undergoing rigid in-plane motions have been studied for flow conditions representative of helicopter rotors, in the remainder of this section results from this study are presented.

Fully turbulent Navier-Stokes calculations were performed on a fine grid containing 259 points in the streamwise direction (200 on the aerofoil) and 96 grid points in the normal direction for a NACA 0012 aerofoil undergoing in-plane motions described by $M_\infty = 0.5113(1 + 0.5263\sin(0.1976t))$, the angle of incidence was 0 degrees and the Reynolds number based upon chord was 1 million. These conditions represent the flow at r/R=0.84 on the rotor blade tested by ONERA[29] at a hover tip Mach number of 0.598 and an advance ratio of 0.45.

Figure (5) shows the unsteady pressure coefficient on the aerofoil at azimuth angles of 30, 60, 90, 120 and 150 degrees. At low azimuth angles the calculated flowfield is dominated by a rapid expansion of the flow at the leading edge, this is a characteristic feature of the relatively blunt NACA 0012 aerofoil. As the freestream Mach number continues to increase a region of high pressure gradient develops towards the trailing edge, this region grows in extent until eventually shock waves form on the aerofoil close to the mid-chord point. The shock waves then migrate towards the trailing edge growing in strength. The maximum Mach number is obtained at 90 degrees azimuth while the maximum shock strength is obtained at an azimuth angle slightly beyond 90 degrees as the flow begins to decelerate. As the flow decelerates further the shock waves move back towards the aerofoil mid-chord point decreasing in strength before finally disappearing.

The importance of dynamic effects can be demonstrated by comparing unsteady pressure distributions at symmetric azimuth angles, i.e. azimuth angles which have the same instantaneous Mach number. For instance, comparing Figures (5d) and (5b) we observe dramatic differences, with and without a shock wave respectively. The influence of flow unsteadiness is further demonstrated when unsteady results are compared with steady calculations performed at the appropriate instantaneous Mach number. In Figure (6) such a comparison is made for azimuth angles of 60 and 120 degrees. From this figure we see that shock strength is reduced when the flow is accelerating, while for decelerating flow dynamic effects are unfavourable.

The flow physics in the unsteady calculations are in good qualitative agreement with experimental observations. There is no suitable experimental data with which the current unsteady computations can be validated, instead comparison is made with three-dimensional rotor tests. In Figure (5) calculated pressure distributions are compared with those obtained in the rotor experiment of ONERA[29]. Agreement is generally good for cases in which there is no shock wave, azimuth angles of 30, 60 and 150 degrees. At 90 degrees azimuth the calculated shock wave appears to be moderately weaker than in the experiment and is located a little further towards the trailing edge. Results at 120 degrees azimuth compare poorly with experiment upstream of the shock wave. The calculated shock wave occurs more than 10% aft of the position recorded in the experiment and is of much greater strength.

A second calculation was performed for the NACA 0012 aerofoil undergoing in-plane oscillations described by M_∞=0.5136(1+0.61sin(0.185t)) with α=0° and Re_c=1 million. The flowfield for these conditions was previously calculated by Lerat and Sides[21] using a two dimensional unsteady Euler code.

Figure (7) shows the time history of lift coefficient for four cycles of the in-plane motion. A fine grid containing 259 grid points in the streamwise direction and 96 grid points in the normal direction was employed. 1080 time steps per cycle were used and the residual was reduced at each time step by at least 2.3 orders of magnitude. Despite the symmetric nature of the current problem, a symmetric aerofoil and α=0°, lift is developed on the aerofoil for azimuth angles in the range 90 to 180 degrees. Although the solution is periodic the lift coefficient changes sign for successive cycles, this suggests that the source of the non-symmetric behaviour alternates between the upper and lower surfaces of the aerofoil.

A major concern was that this behaviour was an artefact of the numerical scheme rather than a true reflection of the flow physics. In order to remove any such doubts the influence of important numerical parameters (convergence tolerance and time step) on the computed solution was investigated, see Figure (8). Over the range considered the convergence tolerance of the linear solver did not appear to have any significant effect. Variations in the computed solution were observed for larger time steps than those used in the current calculations, further reductions in time step beyond that currently employed were found to be unnecessary.

The Euler calculations of Lerat and Sides[21] were performed for one half of the domain with symmetric boundary conditions and consequently the possibility of non-symmetric flow is suppressed. Euler calculations performed with the present method for the whole domain do not exhibit non-symmetric behaviour, this strongly suggests that any such behaviour arises as a consequence of viscous interactions.

Further details of the unsteady flowfield are presented in Figure (9) in which instantaneous density contours are plotted for selected azimuth angles during the fourth cycle of the in-plane motion. As before a region of high density develops over the aerofoil as Mach number is increased. Shock waves develop towards the mid-chord point and begin to move downstream. Figure (9c) shows that at 90 degrees azimuth the flow is largely symmetric. Figure (9d) reveals that by 105 degrees azimuth the flow has become non-symmetric. The boundary layer on the upper surface remains attached, while shock induced separation is indicated on the lower surface. The shock wave on the lower surface begins to move forwards as the flow decelerates and the lower surface boundary layer remains detached. The shock wave on the upper surface continues to move towards the trailing edge for a short period of time. By 120 degrees azimuth both the upper and lower shock waves are travelling towards the leading edge and diminishing in strength. The lower surface shock vanishes shortly after 150 degrees azimuth and by 180 degrees azimuth a largely symmetric flow has been re-established.

The establishment of a non-symmetric flowfield appears to be related to the occurrence of shock induced separation, this explains why such behaviour was not observed in previous Euler calculations at the same flow conditions or in the in-plane calculation presented earlier.

McDevitt and Okuna[31] have reported the occurrence of non-symmetric flow for a stationary NACA 0012 aerofoil at 0 degrees incidence. This behaviour was characterised by periodic fluctuations in force and moment coefficients and was associated with the occurrence of shock induced separation. McDevitt and Okuna determined a boundary beyond which buffeting of this kind will occur. Their measurements indicate that at an angle of incidence of 0 degrees the onset of buffet in steady flow will occur for a Mach number above 0.83. The maximum Mach number attained during the current unsteady calculation was 0.827. Although this Mach number is below that for the onset of buffet it is likely that the unfavourable effects of decelerating flow will lead to a significant increase in shock strength sufficient to cause boundary layer separation. In rotor experiments three dimensional effects are likely to have a strong influence once the flow has separated, the approximation of the rotor by in-plane oscillations will no longer be valid and consequently much poorer agreement between experiment and the current approach would be expected.

In Figure (10) comparison is made between computed pressure coefficients at the mid-chord point and experimental measurements for azimuth angles in the range 0 to 180 degrees. Fair agreement is observed between calculated lower surface pressure coefficients and experiment, while for the upper surface agreement is poor for azimuth angles beyond the onset of shock induced separation. Also included in Figure (10) are the results of Euler calculations performed using the present scheme and that of Lerat and Sides. There is good agreement between both sets of Euler calculations. Also of note is the good agreement between the upper surface pressure coefficients obtained from Navier-Stokes and Euler calculations.

Conclusions

A numerical method for the calculation of the unsteady flowfield around aerofoils undergoing in-plane oscillations has been presented. Calculations of the steady flowfield around an RAE2822 aerofoil and the unsteady self-excited periodic flow around a 14% thick aerofoil have been presented which demonstrate the validity of the current approach. The unsteady aerodynamics of a NACA 0012 aerofoil undergoing in-plane motions representative of the forward flight of helicopter rotor blades were studied. Two calculations have been presented; In the first calculation good qualitative agreement was found between the computed flow physics and those observed in experiments. Fair agreement was also observed between computed and measured pressure distributions over most azimuth angles. For the second case a non-symmetric flowfield was calculated as a result of strong shock-boundary layer interactions. Poor overall agreement between experiment and computation beyond the onset of shock induced separation was observed. It is suggested that the onset of a buffet like unsteady phenomena in the two dimensional calculations, which is suppressed by three dimensional effects in the rotor experiments, explains these discrepancies.

Work is now underway to incorporate a higher order turbulence model into the current code. This should provide more accurate predictions of self-excited flow around bi-convex aerofoils and it is hoped that such changes will provide a firm basis with which to look at the combined translation-pitch oscillations which are representative of the motion of lifting rotor blades.

Acknowledgements

This work is funded by the Engineering and Physical Sciences Research Council (EPSRC) under contract number GR/K31664.

The authors would like to thank Professor B. Richards and Dr K. Badcock of the Department of Aerospace Engineering. Glasgow University and Dr. A. Kokkalis and Mr R. Harris of Westland Helicopters Ltd for their invaluable assistance.

References

1. Carr, L.W., "Progress in analysis and prediction of dynamic stall", J. Aircraft, Vol.25, No.1, January 1988.
2. Carr, L.W. and McCroskey, W.J., "A review of recent advances in computational and experimental analysis of dynamic stall", IUTAM Symposium on Fluid

dynamics at high angle of attack, Tokyo, Japan, September 1992.
3. Ekaterinaris, J., Srinivasan, G. and McCroskey, W.J., "Present capabilities of predicting two-dimensional dynamic stall", AGARD CP-552, October 1994.
4. Chandrasekhara, M. and Carr, L.W., "Compressibility effects on dynamic stall of oscillating airfoils", AGARD CP-552, October 1994.
5. McCroskey, W.J., "Vortex wakes of rotorcraft" AIAA Paper 95-0530, January 1995.
6. Strawn, R.C. and Barth, T.J., "A finite volume Euler solver for computing rotary-wing aerodynamics on unstructured Meshes", Proceedings of the 48th American Helicopter society Forum, Washington, June 1992.
7. Duque, E.P.N., " A structured/unstructured embedded grid solver for helicopter rotor flows", Proceedings of the 50th American Helicopter Society forum, Washington, June 1994.
8. Wake, B.E. and Choi, D., "Investigation of high-order upwind differencing for vortex conservation", AIAA Paper 95-1719 CP, June 1995.
9. Smith, M.J. and Sankar, L.N., "Evaluation of a fourth order compact operator scheme for Euler/Navier-Stokes simulations of a rotor in hover", AIAA Paper 91-0766, January 1991.
10. Steinhoff, J., "Vorticity confinement: A new technique for computing vortex dominated flows", Frontiers of computational fluid dynamics 1994, John Wiley and sons Ltd., 1994.
11. Tijdeman, H., "Investigations of the transonic flow around oscillating aerofoils", NLR TR-77090 U, 1977.
12. Edwards, J.W., Thomas, J.L., "Computational methods for unsteady flows", Chapter 5 Unsteady Transonic Aerodynamics, Ed. by D. Nixon, Progress in Astronautics and Aeronautics, Vol. 120, 1989.
13. McDevitt, J.B., Levy, L.L., and Deiwert, G.S., "Transonic flow about a thick circular arc aerofoil", AIAA Journal, Vol. 14, No. 5, May 1976.
14. Mabey, D.G., Welsh, B.L., Cripps, B.E., "Periodic flows on a rigid 14% thick biconvex wing at transonic speeds", RAE TR 81059, May 1981.
15. Levy, L.L., "Experimental and computational steady and unsteady transonic flows about a thick aerofoil", AIAA Journal, Vol. 16, No. 6, June 1978.
16. Rumsey, C., Sanetrik, M., Biedron, R., Melson, N., and Parlette, E., "Efficiency and accuracy of time accurate turbulent Navier-Stokes calculations", Computers and Fluids, Vol.25, No. 2, February 1996.
17. Favier, D., Agnes, A., Barbi, C., and Maresca, C., "Combined translation/pitch motion: A new airfoil dynamic stall simulation", Journal of Aircraft, Vol. 25, No. 9, September 1988.
18. Favier, D., Belleudy, J., Maresca, C., "Influence of coupling incidence and velocity variations on the airfoil dynamic stall", Proceedings of the 48th American Helicopter Society Forum, Washington, June 1992.
19. Favier, D., Berton, E., Pascazio, M., Wang, C.M., Tullahoma, T. and Steinhoff, J.S., "Experimental and numerical investigation of airfoil dynamic stall in combined pitch-translation oscillation", AIAA Paper 95-0310, January 1995.
20. Van der Wall, B.G. and Leischman, J.G., "Influence of variable flow velocity on unsteady airfoil", Proceedings of the 18th European Rotorcraft Forum, September 1992.
21. Lerat, A. and Sides, J., "Numerical simulation of unsteady transonic flows using the Euler equations in integral form", ONERA TP-79-10, February 1979.
22. Habibie, I., Laschka, B. and Weishaupl, C., "Analysis of unsteady flows around wing profiles at longitudinal accelerations", ICAS Paper 94-2.8.1, 1994.
23. Lin, C.Q., Pahlke, K., "Numerical solution of Euler equations for aerofoils in arbitrary unsteady motion", Journal of the Royal Aeronautical Society, June 1994.
24. Osher, S. and Solomon, F, "Upwind difference schemes for hyperbolic systems of conservation laws", Mathematics of Computation, Vol. 38, No. 158, April 1982.
25. Qin, N., "A comparative study of two upwind methods as applied to Navier-Stokes equations for resolving boundary layers in viscous flows.", Glasgow University Report AERO-9120, 1991.
26. Saad, Y., and Schultz, M.H., "GMRES: A generalised minimum residual algorithm for solving non-symmetric linear systems", SIAM Journal of Science, Statistics and Computing, Vol. 7, No. 3, 1986.
27. Badcock, K.J. and Richards, B.R., "Implicit methods for the Navier-Stokes Equations", AIAA Journal, March 1996.
28. Cook, P., McDonald, M., and Firmin, M., "Aerofoil RAE 2822 - Pressure distribution and boundary layer wake measurements", AGARD R-138, 1979.
29. Tauber, M.E., Chang, I.C., Caughey, D.A. and Phillipe, J.J., "Comparison of calculated and measures pressures on straight and swept tip model rotor blades.", NASA TM 85872, December 1983.
30. Wake, B.E. and Sankar, L.N., "Solution of the Navier-Stokes equations for the flow about a rotor blade", Journal of the American Helicopter Society, April 1988.
31. McDevitt, J.B. and Okuno, A.F., "Static and dynamic pressure measurements on a NACA 0012 aerofoil in the Ames high Reynolds number Facility", NASA Technical Paper TP-2485, June 1985.

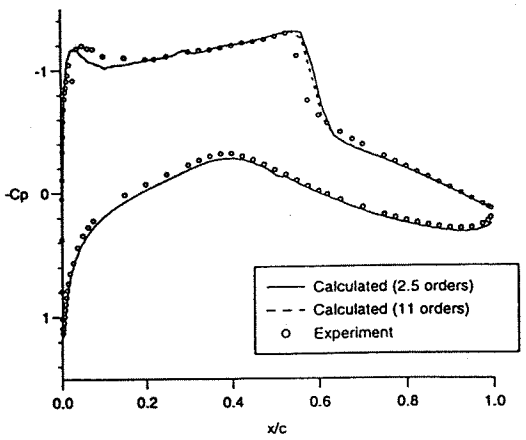

Figure (1) RAE 2822 Aerofoil: α=2.79°,M_∞=0.73, Re_c=6.5 million.

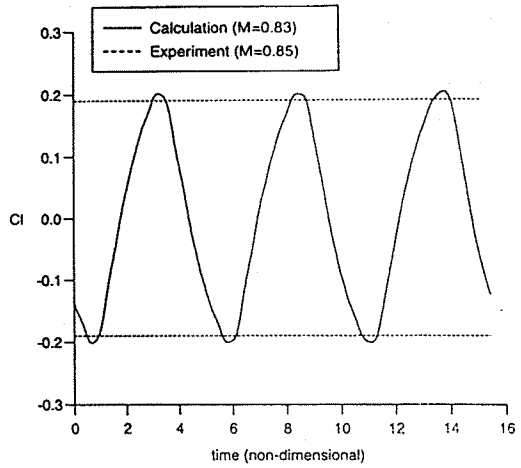

Figure (2) 14% thick bi-convex circular arc aerofoil: α=0.0°,M_∞=0.83, Re_c=7.0 million.

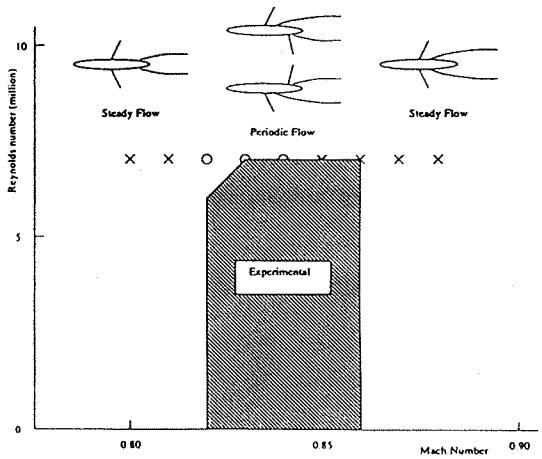

Figure (3) 14% thick circular arc aerofoil: measured and calculated boundaries for periodic flow.

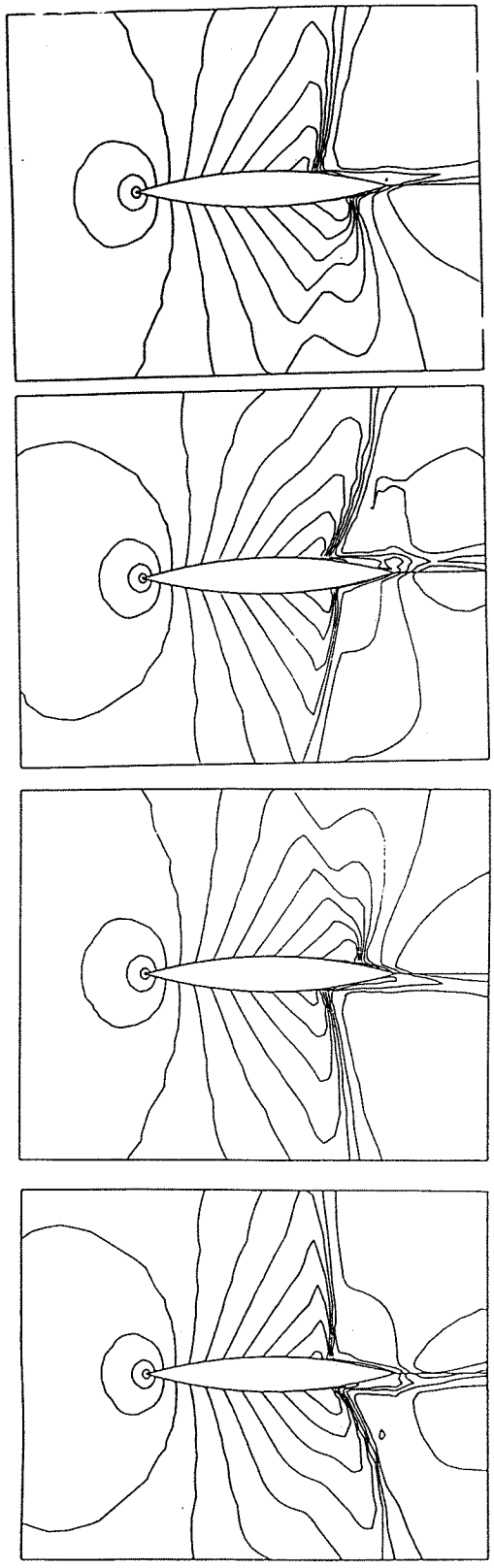

Figure (4) 14% thick bi-convex circular arc aerofoil: calculated instantaneous density contours.

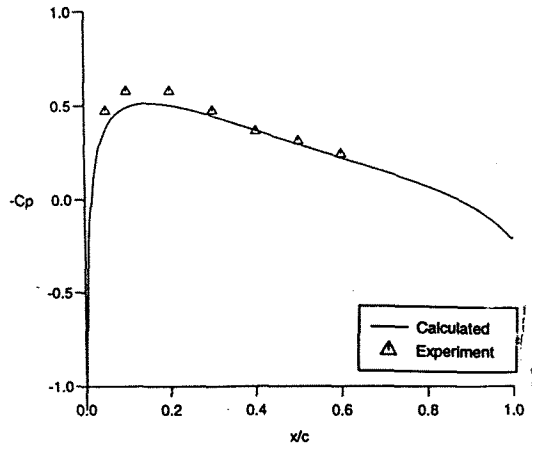

(a) ψ = 30 degrees.

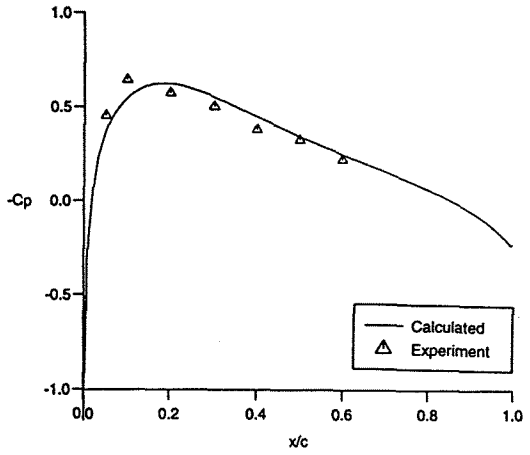

(b) ψ = 60 degrees.

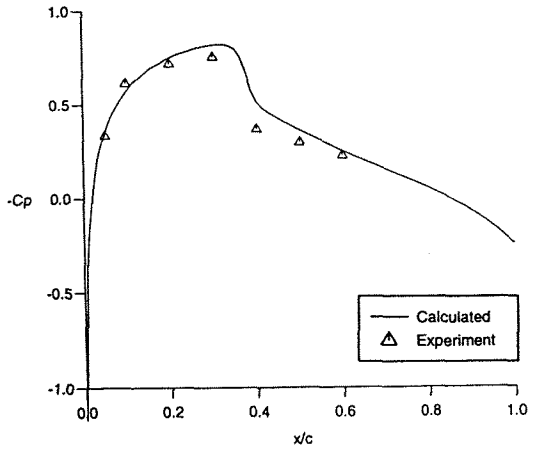

(c) ψ = 90 degrees.

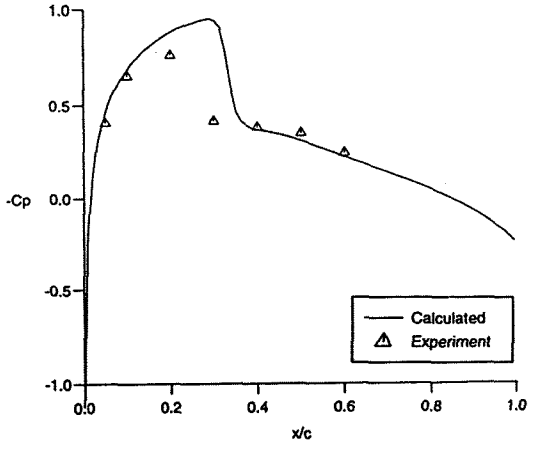

(d) ψ = 120 degrees.

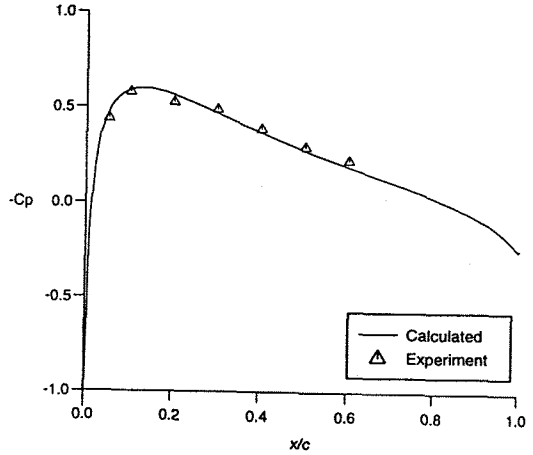

(e) ψ = 150 degrees

Figure (5) NACA 0012 aerofoil: α=0°, Re_c = 1 million, M_∞=0.5113(1+ 0.5263sin(0.1976t)).

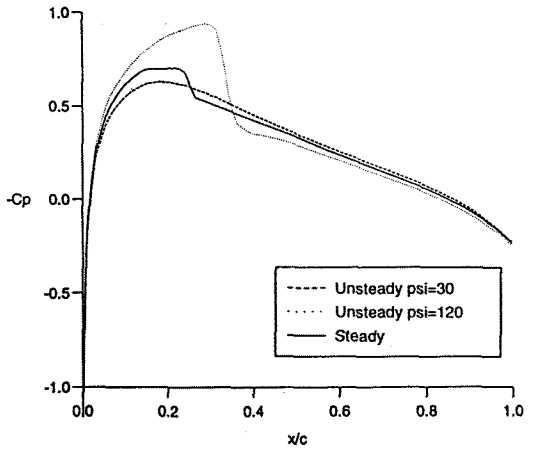

Figure (6) Comparison of steady and unsteady calculations.

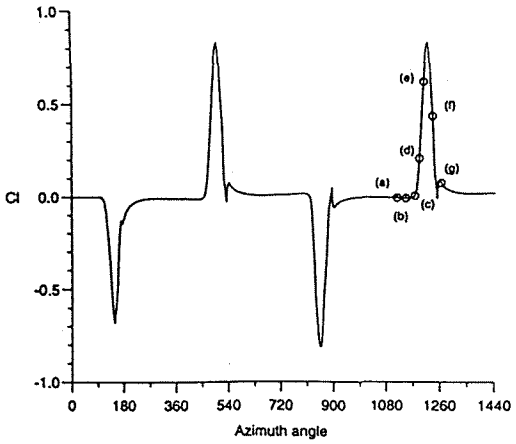

Figure (7) NACA 0012 aeofoil, Re_c= 1 million, M_∞=0.5136(1+0.61sin(0.185t)): Time history of C_L.

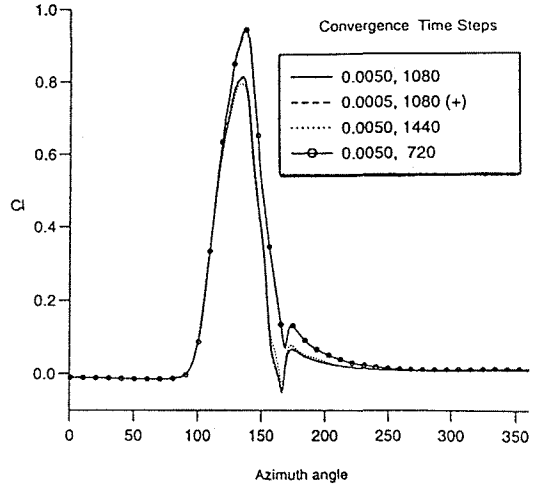

Figure (8) NACA 0012 aeofoil: Influence of time step and covergence on calculated result.

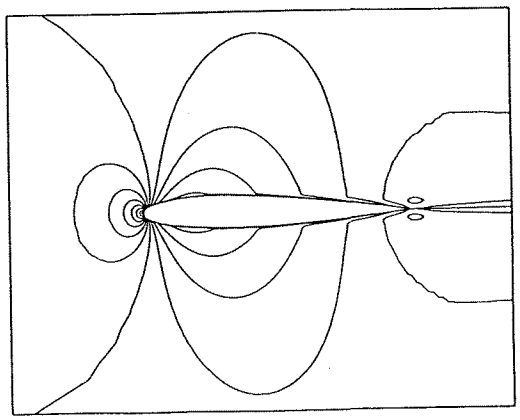

(a) $\psi = 30°$

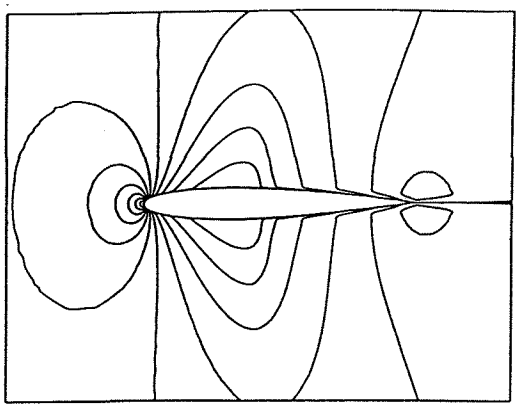

(b) $\psi = 60°$

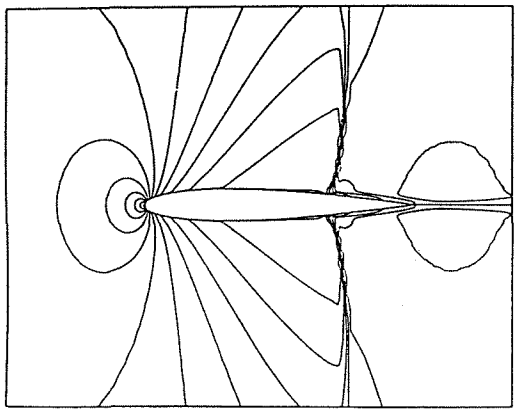

(c) $\psi = 90°$

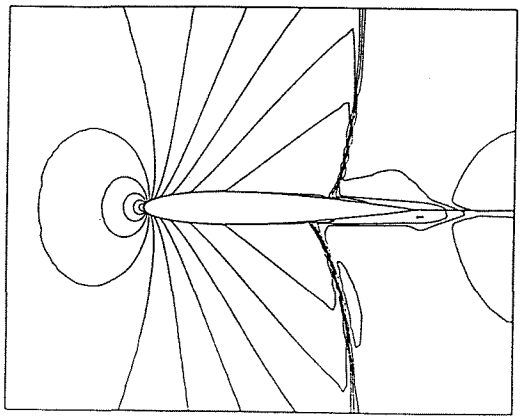

(d) $\psi = 105°$

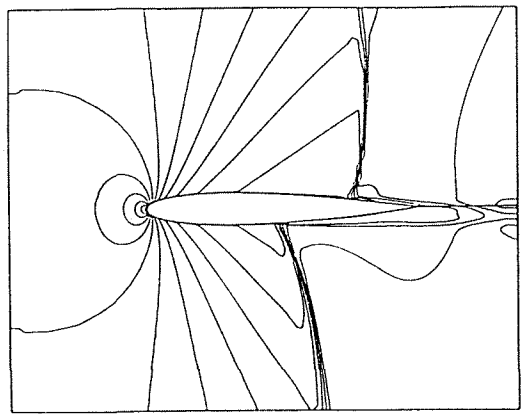

(e) $\psi = 120°$

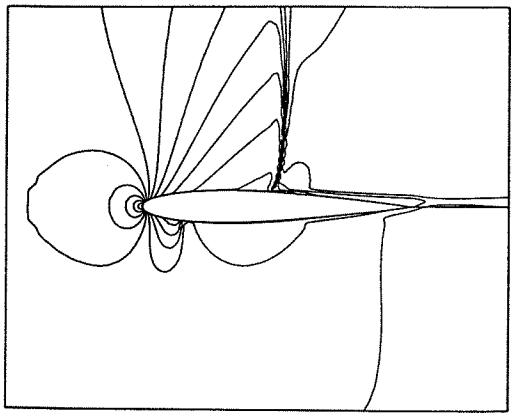

(f) $\psi = 150°$

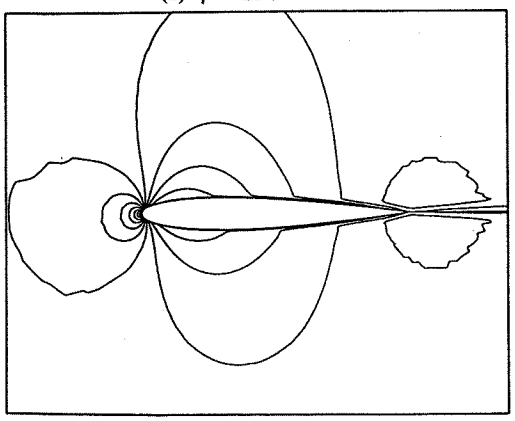

(g) $\psi = 180°$

Figure (9) NACA 0012: Instantaneous density contours for selected azimuth angles.

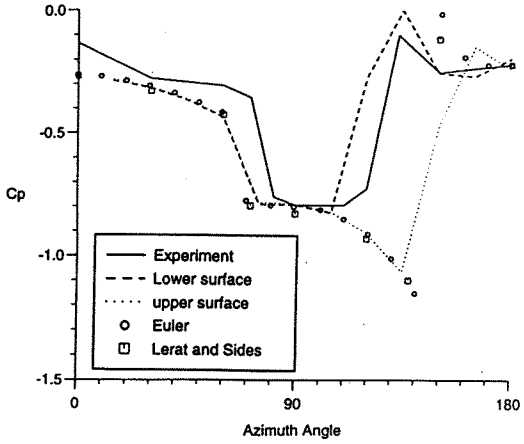

Figure (10) NACA 0012: Comparison of measured and computed pressure coefficients at x/c=0.5.